ADVANCED FUNCTIONAL MATERIALS
www.afm-journal.de

Synthesis of Alternating Copolysiloxane with Terthiophene and Perylenediimide Derivative Pendants for Involatile WORM Memory Device

Guanyin Wen, Zhongjie Ren, Dianming Sun, Tingjie Zhang, Lili Liu, and Shouke Yan**

Alternating copolysiloxane with both electron donor terthiophene and electron acceptor perylenediimide derivative pendants (PTSi-alt-PDISi) is synthesized successfully. The polymer exhibits high decomposition and glass transition temperatures, good film-forming ability, and high morphological stability. The estimated HOMO and LUMO energy levels of PTSi-alt-PDISi are –5.77 and –3.90 eV, respectively. The fabricated memory device with the configuration of ITO/PTSi-alt-PDISi/Au(Al) shows nonvolatile write-once-read-many-times (WORM) memory characteristics. Its turn-on threshold voltage is 1.7 V, while its ON/OFF current density ratio is around 10^4 in ambient atmosphere. The well-defined memory property of PTSi-alt-PDISi is attributed to the transition of the pendant terthiophene and perylenediimide groups from the disoriented state to the ordered face-to-face conformation at the threshold voltage and the charge transfer interaction between pendent terthiophene donor and perylenediimide acceptor moieties, which are confirmed by XRD patterns and fluorescence emission measurement. This suggests that the new donor–acceptor polysiloxanes have potential applications in the field of memory devices.

1. Introduction

The availability of both n-type (electron acceptor) and p-type (electron donor) conductors is essential for diodes and complementary circuits, structures offering high operating speeds and low power consumption.[1–4] In recent years, tremendous effort has been devoted to donor–acceptor polymers for memory device application because of their flexible device structure, low cost, solution processibility, and three-dimensional stacking capability.[5–7] Donor–acceptor polymers include both electron donor and acceptor moieties within a repeating unit, which can be switched between two conductive states under a threshold voltage. The design and synthesis of processable donor–acceptor polymers with good chemical, mechanical, and morphological properties, which can provide the necessary electronic properties within a single macromolecule, is desirable for memory device applications. They have significant advantages over inorganic silicon- and metal-oxide-based memory materials.[8–11] These semiconducting properties of donor–acceptor polymers can be derived either by conjugation of the polymeric backbone (main chain polymers) or by attaching donor–acceptor molecular pendants to the backbone (pendant polymers). Several kinds of main chain polymers[10,12,13] and pendant polymers[14,15] have been reported for the volatile and nonvolatile memory devices. For example, functional polyimide derivatives (PI) is one kind of most extensively studied main chain donor–acceptor polymers due to the excellent thermal stability, chemical resistance, mechanical strength, and high ON/OFF current ratio resulting from the low conductivity in the OFF state. It was demonstrated that the PI derivatives containing electrondonating carbazole or triphenylamine moieties can be used for devices of dynamic random access memory (DRAM), static random access memory(SRAM), write-once-read-many times (WORM) and flash memory via an external voltage bias or pulse.[16–21] Compared to the main chain donor–acceptor polymers, the studies on pendant polymers for memory devices are relatively less. Chen et al. have reported the synthesis and resistive-type switching memory characteristics of random copolymers with pendent triphenylamine and 1,3,4-oxadiazole.[22] Kang et al. have fabricated nonvolatile WORM memory device based on anacrylate polymer with electron donating carbazole pendant groups.[23] In addition, Huang et al. constructed a supramolecular organic semiconductor for nonvolatile flash memory cell by incorporating nonplanar phenylfluorene moieties into PVK using Friedel-Crafts postfunctionalization of PVK.[24] However, most of these donor–acceptor polymers have aliphatic hydrocarbon backbones with low dimensional stability as well as high ON and OFF switching voltages.[25–28] Thus, it remains a great challenge to develop highly stable nonvolatile memory devices based on high performance polymers.

The polysiloxane is a versatile polymer with good solubility in common organic solvents, good film-forming ability, fair adhesion to various substrates,[29,30] and excellent resistances to

G. Wen, Prof. Z. Ren, D. Sun, T. Zhang,
L. Liu, Prof. S. Yan
State Key Laboratory of Chemical Resource Engineering
Beijing University of Chemical Technology
Beijing 100029, China
E-mail: renzj@mail.buct.edu.cn;
skyan@mail.buct.edu.cn

DOI: 10.1002/adfm.201304004

thermal, chemical, and irradiation degradation[31] that render it particularly attractive for use in a variety of optoelectronic applications. Therefore, development of easily synthesized polysiloxanes with efficient donor–acceptor pendant groups could be one of the most promising pathways to achieve high stable nonvolatile memory devices. To our knowledge, polymer with siloxane main chain for memory devices has not been reported yet.

Perylenediimide (PDI) derivatives are a particularly interesting class of electron acceptors. They have high molar absorption coefficient in the visible and high electron mobilities in n-type organic field-effect transistors.[32–34] Additionally, the low HOMO energy of most PDI derivatives facilitate the hole transfer to the conjugated polymer after absorption of light by the PDI molecule and the excited state of the PDI can be transferred to the donor polymer depending on the driving force of the processes. Moreover, PDI derivatives also display excellent photochemical and thermal stability.[35] Taking these distinctive natures of perylenebisimide into account, the incorporation of PDI into donor–acceptor polymers as an electron acceptor is confirmed to be effective stabilizing radical anion induced by charge transfer (CT) from donor to acceptor, resulting in nonvolatile memory characteristics with a stable CT state. Furthermore, Ueda et al. have confirmed that the tunable electrical bistability from the volatile to nonvolatile WORM memory characteristics was obtained by introducing increased PDI composition into polyimide.[36]

Herein, we have designed and successfully synthesized a donor–acceptor alternating copolysiloxane (PTSi-alt-PDISi) by incorporating good electron-donor terthiophene and electron-acceptor PDI derivative units into a polysiloxane backbone. For comparison, two terthiophene and PDI derivatives based homo-polysiloxane (PTSi and PDISi) were also synthesized and characterized. The memory behaviors of PTSi-alt-PDISi was characterized by a simple sandwich device of spin-coated PTSi-alt-PDISi film between ITO and Au or Al electrode, which displays nonvolatile WORM memory characteristics. This may provide a new strategy for designing polysiloxane-based memory device materials.

2. Results and Discussion

2.1. Synthesis and Characterization

Synthetic routes of PTSi, PDISi and PTSi-alt-PDISi are shown in **Scheme 1**. The precursor 5-bromo-5′-methy-2,2′;5′,2″-terthiophen was synthesized according to the previous literature.[37] The compound **1** could be easily obtained by Barbier-Grignard reaction of 5-bromo-5″-methy-2,2′;5′,2″-terthiophen and methyldiethoxylchlorosilanes with magnesium under the reflux condition. ^{1}H-NMR spectrum of compound **1** shows a new peak at 3.8 ppm, assigned to the proton of the Si-OCH_2 groups, suggesting the successful preparation of **1**. **2** was obtained by hydrolysis of **1** in a dilute THF–HCl solution under 0 °C. Low temperature could suppress the undesired condensation between the formed silanols. ^{1}H-NMR spectrum of **2** shows a new peak at 5.75 ppm, assigned to the proton of the Si-OH groups, and the peak at 3.8 ppm assigned to the protons of Si-OCH_2 disappears, indicating the complete hydrolysis of **1**. **3** were synthesized by simple conversion of 1,6,7,12-tetrachloroperylene-3,4,9,10-tetracarboxylic acid dianhydride with a mixture of octyl amine and 3-aminopropyldiethoxylmethylsilane with a yield 34%. **4** was hydrolyzed into **3** with the similar condition of **1** hydrolysis as confirmed by ^{1}H-NMR. The desired polymers PTSi, PDISi, and PTSi-alt-PDISi were easily synthesized from corresponding diethoxy monomer (OEt-Si) and dihydroxy monomer (OH-Si) under tetrabutyl titanate

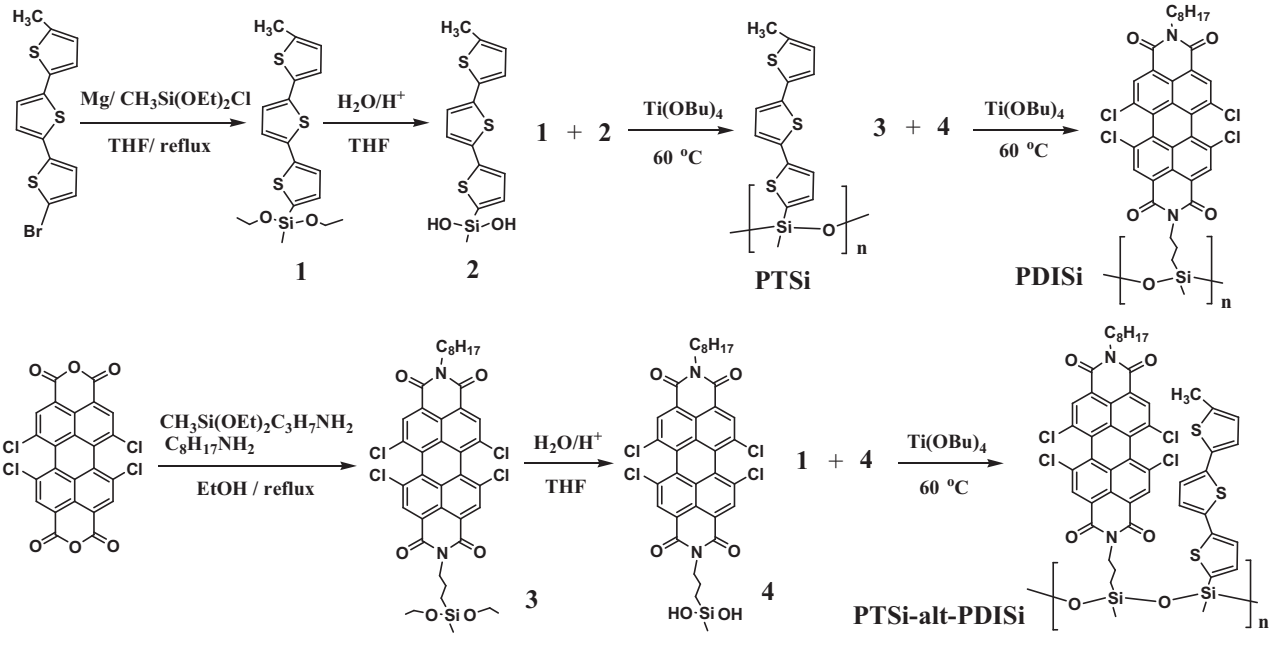

Scheme 1. synthetic routes of PTSi, PDISi and PTSi-alt-PDISi.

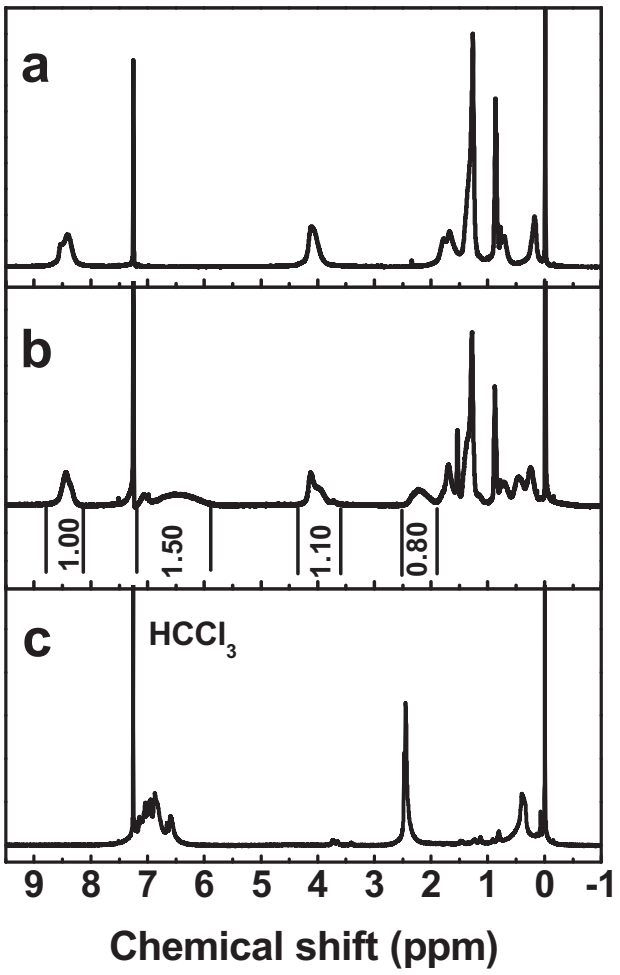

Figure 1. ^{1}HNMR spectra of a) PDISi, b) PTSi-alt-PDISi, and c) PTSi.

(TBOT) catalyzed polycondensation for polysiloxanes as shown in Scheme 1. In ^{1}H-NMR of PTSi and PDISi (**Figure 1**), the peak assigned to proton of Si-OH groups disappears, indicating complete polymerization of Si-OH groups. As shown in Figure 1b, for PTSi-alt-PDISi, there appears the characteristic peaks at 8.2–8.7, 6–7.2, 3.8–4.3, and 2–2.5 ppm assigned to the protons of aromatic ringin PDI block, aromatic ring in terthiophen block, NH in PDI block and $-CH_3$ in terthiophen block, respectively. In addition, the reasonable ratio of peak area of these protons also suggested PTSi-alt-PDISi were obtained as the desired structure successfully. The target polymer PTSi, PDISi. and PTSi-alt-PDISi solubility test found that they are readily soluble in toluene, THF, dichloromethane, and so forth. The weight average molecular weight (Mw) of PTSi, PDISi, and PTSi-alt-PDISi was determined to be 15.2 kDa, 27.7 kDa, and 10.5 kDa with PDI 1.16, 1.25, and 1.30 respectively by GPC in THF with polystyreneas standard. (see Figure S1 in Supporting Information).

To confirm the alternate polymerization of terthiophen and perylene diimide units in PTSi-alt-PDISi, the matrix-assisted laser desorption ionization mass spectroscopy (MALDI-TOF MS) of PTSi-alt-PDISi was performed as shown in **Figure 2**. We could obtain convincing structure information from it. The

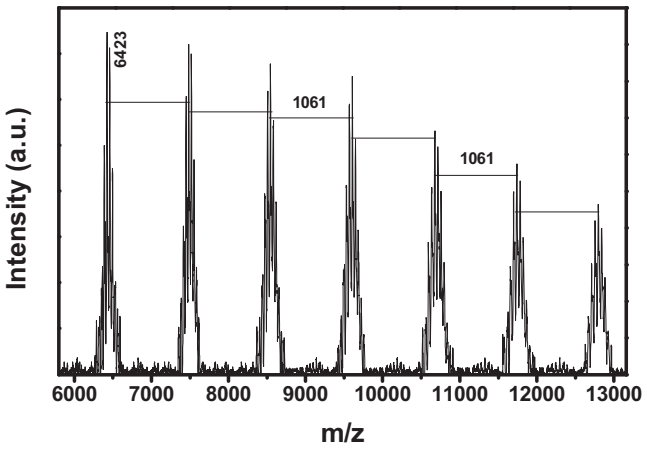

Figure 2. MALDI-TOF-MS of PTSi-alt-PDISi.

spectrum bears the characteristic shape of an alternating condensation polymer, which is made up of clusters of isotopic peaks. The nominal separation between these alternate major clusters, 1061 Daltons, is exactly equal to the repeat unit of terthiophen and perylene diimide moieties, indicating that the synthesis proceeded as expected to give a alternating structure without a side reaction.

2.2. Thermal Properties

The thermal properties of PTSi, PDISi and PTSi-alt-PDISi were determined by differential scanning calorimetry (DSC) and thermogravimetric analysis (TGA). The introduction of perylenediimide blocks increased the decomposition temperature (T_d) of PTSi-alt-PDISi and the temperature with 5 wt% weight loss of the initial amount is at ≈ 379 °C, showing the excellent thermal stability (Figure S2, Supporting Information). DSC was performed under nitrogen atmosphere with a heating rate of 10 °C min^{-1}. As shown in **Figure 3**, the distinct glass transition temperature (T_g) is observed at 80 °C, 196 °C, and 132 °C for PTSi, PDISi, and PTSi-alt-PDISi, respectively. No crystallization and melting peaks is obtained, indicating an amorphous feature of the product. High T_g of PTSi-alt-PDISi may attribute to the polysiloxanes skeleton and introduction of PDI blocks. The high T_d and T_g of the pendent donor–acceptor copolymers particularly suggest their long-term stability of device operation.

2.3. Photophysical Properties

The UV-visible absorption spectra of PTSi, PDISi, and PTSi-alt-PDISi in thin films are shown in **Figure 4**. The absorption spectrum of PDISi exhibits the characteristic fingerprint vibronic fine structure of PDI with the peaks at 519, 486, 426, and 278 nm, respectively. The optical band gap is 2.0 eV calculated from the onset of optical absorption. PTSi in dichloromethane solution features peak at 365 nm attributed to terthiophene groups, while a shoulder peak at 408 nm may reflect the strong π–π interactions between molecular chains.

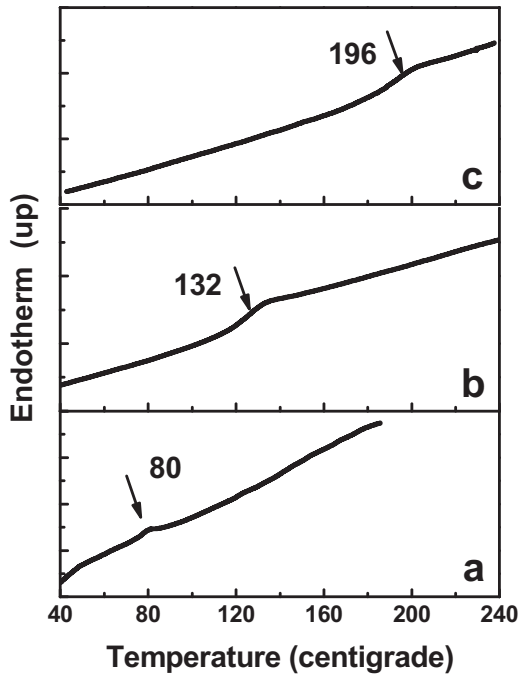

Figure 3. DSC traces of a) PTSi, b) PTSi-alt-PDISi, and c) PDISi.

The absorption spectrum of PTSi-alt-PDISi displays characteristic peaks of PTSi and PDISi. However, comparing with the peaks of PTSi and PDISi, all peaks shows bathochromic shift in PTSi-alt-PDISi. Thiophene absorption peaks shift from 364 nm to 375 nm and perylene bisimide absorption peaks at 519 nm shift to 523 nm, indicating the absorption areas spectrum was enhanced.

2.4. Electrochemical Properties

The electrochemical behavior of PTSi, PDISi, and PTSi-alt-PDISi were investigated by cyclic voltammetry (CV). CV

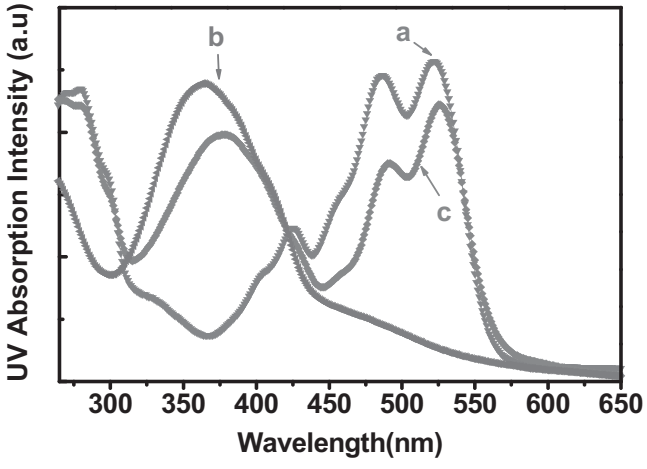

Figure 4. UV-Vis spectra of a) PDISi film, b) PTSi film, c) PTSi-alt-PDISi film.

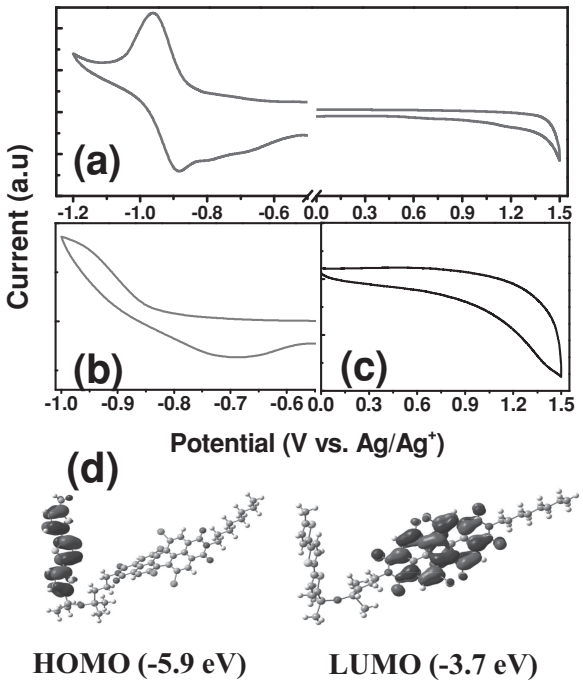

Figure 5. The cyclic voltammograms of a) PTSi-alt-PDISi, b) PDISi, c) PTSi, d) HOMO and LUMO levels of PTSi-alt-PDISi caculated by Gaussian 03.

experiment was carried out in degassed anhydrous acetonitrile solution. PTSi-alt-PDISi shows reversible oxidation and reduction processes in the performed potential range (**Figure 5**), suggesting reversible electrochemical doping and dedoping behaviors during potential sweeps, which is desirable for charge and hole transporting materials. HOMO and LUMO energy levels of PTSi-alt-PDISi were calculated according to the inner reference ferrocene redox couple $E^0 = (F_c/F_c^+) = +0.41$ V versus Ag/Ag^+ in acetonitrile by using the formula $E_{HOMO} = -e\,(E_{ox} - E_{Fc}) + 4.8$. The HOMO and LUMO energy levels of PTSi-alt-PDISi were calculated to be –5.77 and –3.90 eV, respectively, and electrochemical band gap was 1.87 eV. PTSi displays only oxidation process and its HOMO energy level was calculated to be –5.46 eV. In addition, band gap (E_{gap}) estimated from UV absorption spectrum is about 2.25 eV, and then LUMO energy level was calculated to be –3.21 eV according to LUMO = HOMO – E_{gap}. PDISi shows only reduction process and the HOMO and LUMO energy levels were calculated to be –3.95 and –5.95 eV, respectively. We could deduce that the HOMO and LUMO of PTSi-alt-PDISi copolymer depend on its block thiophene and perylene bisimide, respectively. A slight shift of HOMO and LUMO may be caused by the interaction between the donor and acceptor blocks.

Molecular simulation of the basic unit of PTSi-alt-PDISi was carried out at the DFT B3LYP/3–21G level with the Gaussian 03 program package. Figure 5d shows the resulting HOMO and LUMO of PTSi-alt-PDISi. The HOMO is located mainly on the block thiophene moieties, whereas the LUMO is located on the block PDI moieties, indicating that in the copolymer, the terthiophene moieties act as the electron donors and the PDI moieties act as the electron acceptors. The calculated

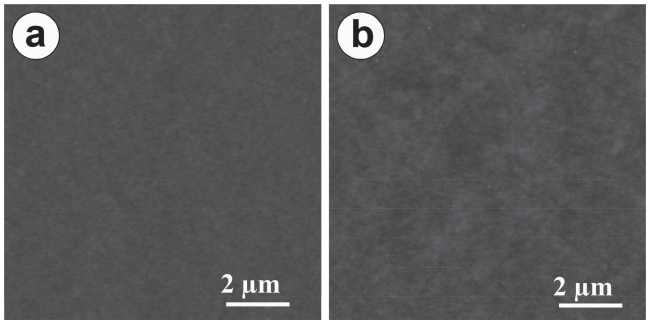

Figure 6. AFM topographic images of the solution processed PTSi-alt-PDISi films a) before and b) after annealed at 200 °C for 2 h.

energy levels are comparable to the HOMO and LUMO energy levels of PTSi-alt-PDISi, measured by cyclic voltammetry.

2.5. Morphology Properties

The film-forming ability, morphological stability of PTSi-alt-PDISi were investigated by the atomic force microscopy (AFM). As shown in **Figure 6**a, the AFM image of PTSi-alt-PDISi film displays smooth and homogeneous morphology with small values of root-mean-square (RMS) roughness of 0.29 nm. It is free of particle aggregation or phase separation, suggesting the good film forming ability. Moreover, the surface roughness was nearly unchanged after annealed at 200 °C for 24 h (Figure 6b). The excellent stability of film morphology appears to be a result of the polysiloxane backbone, which should be capable of keeping films integrity throughout the fabrication and operation process. Good film-forming ability, high stability and good adhesion to ITO electrode may be conducive to reduce the interfacial energy barrier, and thus gives easy access for further improvement of the electronic properties.

2.6. Electrical Properties

The electrical behaviors were tested by the current density–voltage (*J–V*) characteristics on the ITO/polymers/Au sandwiched device. The structure of device is shown in **Figure 7**a. The memory device based on the mixture of PTSi and PDISi has not been conducted because the low thermal degradation temperature of PTSi. Figure 7b shows the typical *J–V*

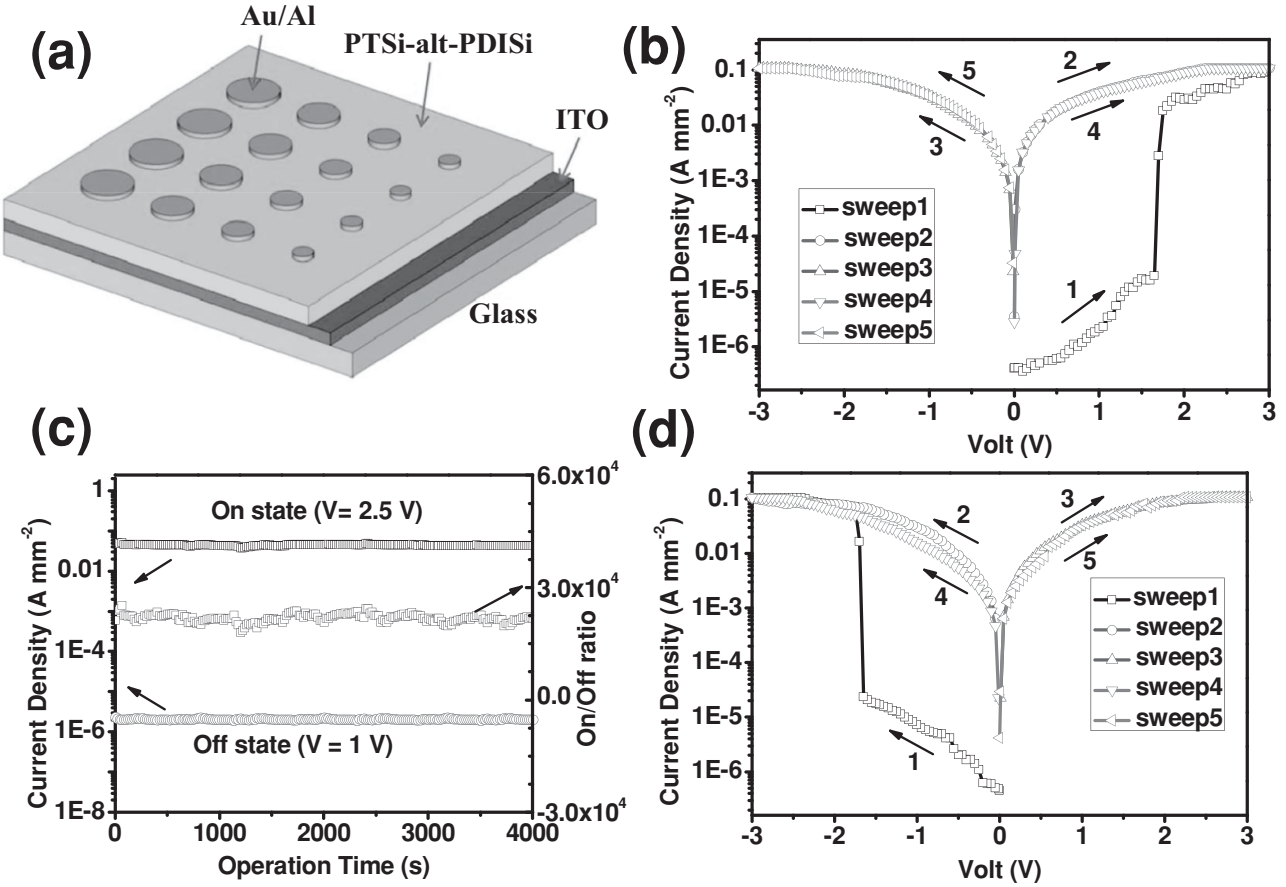

Figure 7. a) The illustrative structures for the ITO| PTSi-alt-PDISi (45 nm)|Au sandwich memory device; b) *J–V* characteristics of the memory device; the sweep sequence and direction are indicated by the numbers and arrows, respectively (sweep numbers 1, 2, and 4: 0 to +3 V; sweep numbers 3 and 5: 0 to –3 V); c) Effect of operation time on the current density of the sandwich device at the ON and OFF states; d) *J–V* characteristics of the memory device, sweep numbers 1, 2, and 4: 0 to –3 V; sweep numbers 3 and 5: 0 to +3 V.

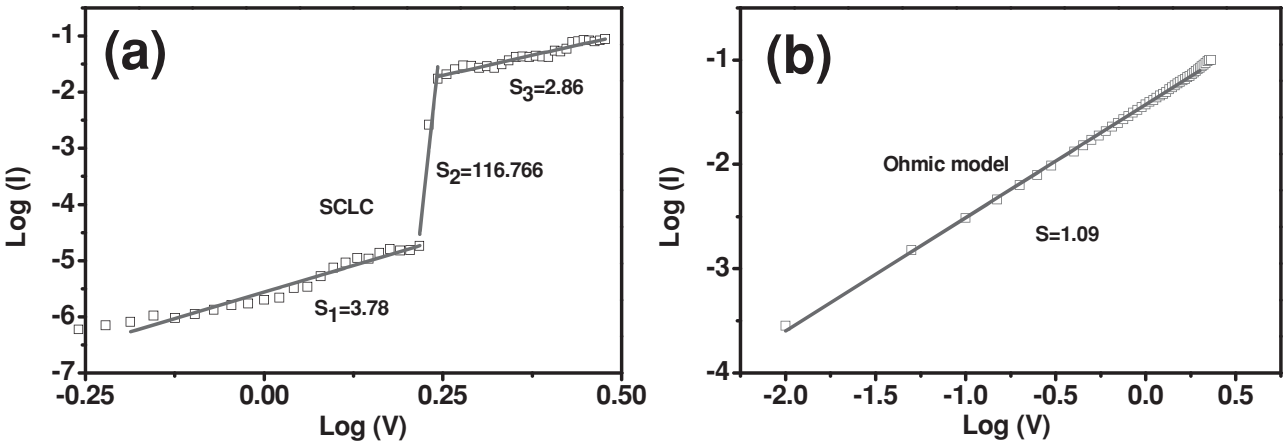

Figure 8. Experimental and fitted *I–V* curves of the ITO/ PTSi-alt-PDISi /Au memory devices a) OFF state and b) ON state.

characteristics of a bistable memory device of PTSi-alt-PDISi. In the first positive sweep from 0 to 3 V (ITO: cathode; Au: anode), an abrupt increase in current density was observed at a switching threshold voltage of about 1.7 V, indicating the device transition from a low-conductivity state (OFF) to a high-conductivity state (ON). After this transition, the device remained in its high-conductivity state during the subsequent positive scan (the second sweep). The subsequent negative scan from 0 to 3 V (the third sweep) did not turn the device from the ON to OFF state, and the device kept its high-conductivity state during the following forward scan (sweep 4 from 0 to 3 V) and reverse scan (sweep 5 from 0 to 3 V). This indicates that the OFF-to-ON transition is irreversible. Once the device is switched to its high conductivity state, it remains there and cannot be retrieved to its initial low conductivity state. Subsequent measurement shows that the device further remained in the ON state after turning off the power, implying its nonvolatile features. According to the literature,[38] devices with such electrical characteristics can serve as write-once-read-many-times (WORM) memory in digital information storage. The OFF-to-ON electrical switching process is equivalent to the ''writing'' process in a traditional memory cell. The distinct bielectrical states in the voltage range of 0 to 1.7 V allowed a voltage (e.g., 1.0 V) to read the "0" or "OFF" signal (before writing) and "1" or "ON" signal (after writing) of the memory. Further experiments on duplicated devices revealed that the *J–V* characteristics were repeatable with good accuracy, and device degradation was not observed.

In addition, Figure 7c shows the stability of the device and the ON/OFF current density ratio as a function of operation time. Under a constant bias of 1 V, the device exhibits a stable current of about 10^{-5} A. mm^{-2} (OFF state). When a bias of 2.5 V was applied, the device was kept at its ON state with a current of about 10^{-1} A mm^{-2}. No significant decrease in current density was observed at the ON state with longer operation time, the device maintained an ON/OFF current density ratio of as high as 10^4.

Similar ON and OFF switching behaviors were observed for the device when sweeping with a negative voltage (Figure 7d). These results indicate that the PTSi-alt-PDISi film in the device exhibits excellent unipolar ON and OFF switching behaviors regardless of the sweep direction (i.e., independent of polarity). In addition, Similar switching performances were observed using an evaporated aluminum-top electrode (see Supporting Information Figure S15a,b). Moreover,when the film thickness increases from 45 nm to 155 nm, the bistable electrical states could not be observed and the device is electrically insulating during the voltage sweeping process (Supporting Information, Figure S15c). This result allows the exclusion of interfacial oxides, metal nanoparticles, or filaments as the origin of the observed conductance switching.[39] Furthermore, the almost linear current-area dependence of both the OFF and ON states when the active device area was reduced from 0.16 to 0.04 to 0.0225 mm^2 (Au electrode), giving almost constant current densities, indicate the absence of sample degradation and dielectric breakdown. The conductance switching observed can thus be fully attributed to the change in the material properties of the polymer PTSi-alt-PDISi layer upon applying an external bias.

To investigate the carrier transport mechanism of the devices based on PTSi-alt-PDISi active layer, we analyzed the *I–V* characteristics of the OFF and ON states, as shown in **Figure 8**. The trap-limited space charge limited conduction (SCLC $I \approx V^{m+1}$ ($m > 1$)) model was found to satisfactorily fit the *I–V* data for the OFF state. This result indicates that a trap-limited SCLC mechanism is dominant in the OFF state of the PTSi-alt-PDISi film. On the other hand, for the ON state, the logarithmic plot of the *I–V* data is shown in Figure 8b, the obtained slope is nearly equal to 1, indicating that Ohmic conduction is dominant when the device is in the ON state.

According to the operating mechanism of the PTSi-alt-PDISi based memory device, electrical field induced conformation change and the charge transfer interaction between pendent terthiophene donor and perylenediimide acceptor moieties could explain the electrical switching behavior of PTSi-alt-PDISi appropriately. Several literatures have reported the electrical bistability of some non-conjugated polymers with pendant active groups.[40–42] For example, memory effects of PVK derivatives with flexible spacers between the carbazole pendant group and the polymer backbone,[23,39] in which regio-random and regioregular alignments corresponds to the low and high conductivity states, only showed WORM or volatile features.

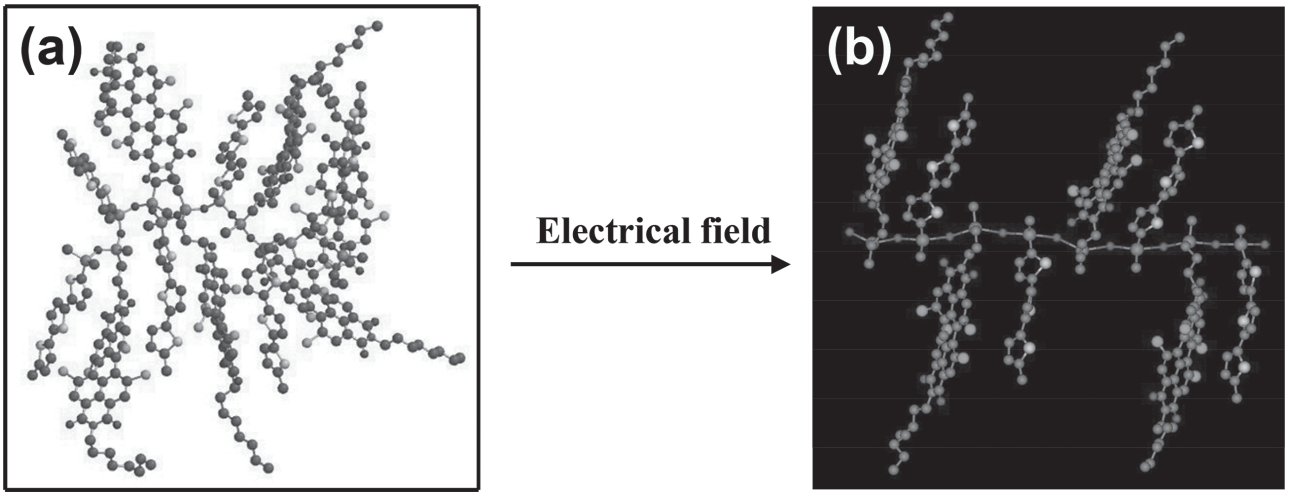

Figure 9. Schematic diagram for the switching transition from low to high conductivity states a) regiorandom geometry of PTSi-alt-PDISi optimized by materials studio and b) depicted regioregular geometries of PTSi-alt-PDISi.

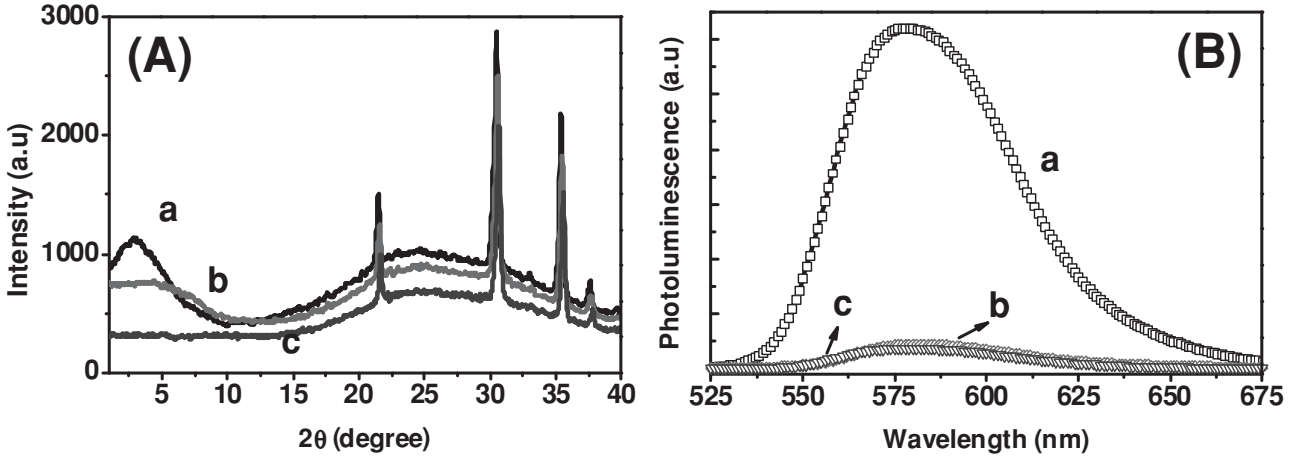

Figure 10. A) XRD patterns of PTSi-alt-PDISi after application of a) 2.5 V bias, b) 0 V bias, and c) ITO glass substrate; B) Fluorescence emission spectra of ITO/PTSi-alt-PDISi/Al devices a) at 0 V, b) after application of 2.5 V bias, and c) after power-off for 30 min.

Similarly, the degree of regioregularity of PTSi-alt-PDISi film would be low at the ground state promoted by the flexible molecular spacer between the side groups and the polymer backbone, which does not favor the charge-transfer (CT) interaction of terthiophene and PDI groups as shown in **Figure 9**a. As a result, the charge carriers experience difficulty in hopping through the neighboring terthiophene and PDI groups because of the absence of face-to-face conformations and the presence of a lengthy distance between the neighboring terthiophene and PDI groups. Therefore, the current of the device based on PTSi-alt-PDISi is low and the device is in its low-conductivity state ("0" state) at low voltage as schematically illustrated in Figure 9a. At the threshold voltage, PTSi-alt-PDISi consists of nearly full face-to-face conformation (Figure 9b), which open a charge transport pathway for hole and electron hopping and then the CT complex is formed, leading to a surge in carrier concentration and current density. The memory devices are therefore transited from the OFF to ON state. The large dipole moments of terthiophene and PDI in PTSi-alt-PDISi probably lead to a stable CT complex,[43,44] which also lead to a highly stable conformation with intrachain alignments. Even the driving power is turned off, the ON state can still remain due to the stability of CT complex. Thus the device displays the non-volatile feature.

The proposed mechanism of conformation change and charge transfer is supported by X-ray diffraction (XRD) and fluorescence emission measurements. XRD patterns of the PTSi-alt-PDISi and ITO glass are shown in **Figure 10**A (diffraction peaks at 2θ around 21.4°, 30.5°, 35.3°, and 37.6° arise from the ITO glass substrate). PTSi-alt-PDISi does not display obvious diffraction peak and only one broad peak at around $2\theta = 2–7^0$ is observed, indicating its amorphous nature. However, it shows a characteristic diffraction peak at $2\theta = 2.9°$ (≈ 3.0 nm) when it is stressed at 2.5 V. Moreover, d-spacing about 3.0 nm, which is nearly consistent with theoretical width of PTSi-alt-PDISi (Figure 9b). The result suggests that the pendant groups in PTSi-alt-PDISi have transformed from a regio-random arrangement, via the field induced conformation change, to

a regio-regular arrangement. In addition, XRD spectrum of PTSi-alt-PDISi remains unchanged when the applied bias was turned off for 30 min, which is consistent with the nonvolatile nature and WORM behavior of the memory device.

The proposed mechanism of conformation change and charge transfer is also supported by fluorescence emission spectra of the PTSi-alt-PDISi films. A removable liquid-Hg droplet was used as the top electrode in place of the Au contacts. After switching the PTSi-alt-PDISi film from the OFF to ON state, the Hg electrode was removed and the resultant polymer film was analyzed by fluorescence emission spectra (λ_{ex} = 510 nm). The PDISi-alt-PTSi film shows broad emission at about 520 nm (Figure 10Ba). The emission maximum intensity of PDISi-alt-PTSi film was strongly quenched compared with its solution in dichloromethane. This phenomenon may reflect CT interaction between terthiophene donor and PDI acceptor groups happened. The film state is more favorable for CT interaction. When fluorescence emission spectra of the PTSi-alt-PDISi films in their pristine states (OFF state) are compared to those after a voltage sweep of 0 to 2.5 V has been applied (ON state), an obvious decrease in intensity and a slight red shift (3 nm) of the emission peak have occurred as a result of the electrical transition (Figure 10Bb). The red-shift is indicative of increased electronic delocalization among the terthiophene donor and PDI acceptor groups in PTSi-alt-PDISi because the polymer backbone is non-conjugated. The decrease in intensity of emission peak suggests CT interaction increase, which would result in strong fluorescence quenching. CT interaction increase may be attributed to the conformational transition of PTSi-alt-PDISi from a regio-random to a regio-regular arrangement. Moreover, the emission spectrum of the PTSi-alt-PDISi remains unvariable when measured 30 min after turning off the power (Figure 10Bc). It can thus be concluded that the voltage-induced conformation change and the formation of a CT complex are probably responsible for the conductance switching effects observed in the memory devices.

3. Conclusions

In summary, we have successfully prepared new donor–acceptor alternating copolysiloxanes containing pendent electron-donating terthiophene and electron-accepting PDI derivatives. The PTSi-alt-PDISi device exhibited nonvolatile WORM switching, with an ON/OFF current density ratio of 10^4. Moreover, the devices show long retention time of at least 4×10^3 s under a constant voltage stress. The conformation change from the regiorandom and regioregular alignments and the charge transfer interaction between pendent terthiophene donor and perylenediimide acceptor moieties explain the memory characteristics of the PTSi-alt-PDISi. Our results open the molecular design of the pendent polysiloxanes with specific functional donor–acceptor chromopheres for advanced memory applications.

4. Experimental Section

Materials: All reagents (Adamas-beta) were commercially available without further purification except for toluene, n-hexane and tetrahydrofuran, which were distilled over sodium and benzophenone before use. Methyldiethoxylchlorosilanes was synthesized according to the literature.[45]

Chracterization: ^{1}H NMR and ^{13}C NMR spectra were measured on a Bruker AV400 (400MHz) spectrometer. Chemical shifts (δ) are given in parts per million (ppm) relative to tetramethylsilane (TMS; $\delta = 0$) as the internal reference. ^{1}H NMR spectra data are reported as chemical shift, relative integral, multiplicity (s = singlet, d = doublet, m = multiplet), coupling constant (J in Hz) and assignment. UV-Vis absorption spectra were recorded on a Hitachi U-2900 recording spectrophotometer. Differential scanning calorimetry (DSC) was performed on a TA Q2000 Differential Scanning Calorimeter at a heating rate of 10 °C min^{-1} from 25 to 200 °C under nitrogen atmosphere. The glass transition temperature (T_g) was determined from the second heating scan. Thermogravimetric analysis (TGA) was undertaken with a METTLER TOLEDO TGA/DSC 1/1100SF instrument. The thermal stability of the samples under a nitrogen atmosphere was determined by measuring their weight loss while heating at a rate of 10 °C min^{-1} from 25 to 800 °C. Cyclic voltammetry (CV) was carried out in nitrogen-purged dichloromethane at room temperature with a CHI 660E voltammetric analyzer. Tetrabutylammonium hexafluorophosphate ($TBAPF_6$) (0.1 M) was used as the supporting electrolyte. The conventional three-electrode configuration consists of a glassy carbon working electrode, a platinum wire auxiliary electrode, and an Ag/AgCl pseudo-reference electrode with ferrocenium-ferrocene (Fc^+/Fc) as the internal standard. Cyclic voltammograms were obtained at scan rate of 100 mV s^{-1}. The onset potential was determined from the intersection of two tangents drawn at the rising and background current of the cyclic voltammogram. MALDI-TOF mass spectrometric measurements were performed on a Bruker Biflex MALDI-TOF mass spectrometer. Gel permeation chromatography (GPC) analysis was carried out on a Waters 515–2410 system using polystyrene standards as molecular weight references and tetrahydrofuran (THF) as the eluent. The morphologies and thickness of the polymer films coated on the ITO substrate were measured using atomic force microscopy (Agilent-5500 AFM) under tapping mode. The current density-voltage (J–V) characteristics of thesandwich devices were recorded by a Keithley 4200 SCS semiconductor parameter analyzer (Keithley, Cleveland, OH) equipped with a Micromanipulator 6150 probe station in a cleanand metallically shielded box in ambient environment. Molecular simulations of the basic unit of PTSi-alt-PDISi were carried out using the Gaussian 03 software package. The molecular orbital and electronic properties were calculated according to density functional theory (DFT). DFT optimizations using the B3LYP functional with the 3–21G basis set. Fluorescence spectra of the polymer film in the bistable electrical states of the ITO/polymer/Al device were measured in situ on a Shimadzu RF-5301PC Spectrofluorophotometer. X-ray diffraction (XRD) measurements were performed on a Bruker D8 Advance diffractometer with Cu Kα radiation 40 kV.

Sandwich Device Fabrication: The sandwich memory devices using the synthesized PTSi-alt-PDISi as the active layer were fabricated by spreading a CH_2Cl_2 solution onto a pre-cleaned indiumtinoxide (ITO) substrate using a spin coater set at 1200 rpm. The ITO conductive glass was precleaned sequentially with water, acetone, chloroform and isopropanol in an ultrasonic bath for 15 min and then dried by a N_2 gun. After keeping in a clean box programmed at constant temperature and humidity for ≈ 4 h, the spin-coated films were thermally treated under vacuum at 40 °C for 2 h to remove the remaining solvent. The thickness of the PTSi-alt-PDISi films on ITO was tuned by the concetration of solution and was determined by AFM. Finally, the sandwich devices (ITO|PTSi-alt-PDISi |Au/Al) were fabricated by vacuum evaporationof a thin Au/Al layer (≈300 nm) through a shadow mask onto the polymer surface as the top electrode.

Synthesis of 1,6,7,12-tetrachloro-N-octadecyl-N′-(diethoxylmethylsilyl) propyl-perylene-3,4, 9,10-tetracarboxylic acid diimide: A mixture of 1,6,7,12-tetrachloroperylene-3,4,9,10-tetracarboxylic acid dianhydride (5.3 g, 10 mmol), 3-aminopropyldiethoxylmethylsilane (1.91 g, 10 mmol), n-octylamine (1.29 g, 10 mmol) and ethanol (150 mL) was heated to 90 °C for 24 h. The solvent was removed by rotary evaporation, and the crude product was purified by chromatography on silica gel

with petroleum ether/dichloromethane (1/1) to give the orange solid (3.2 g, 39%). ^{1}H-NMR (400 MHz; $CDCl_3$; Me_4Si) δH (ppm): 0.15 (s, 3H; $SiCH_3$), 0.75 (t, J = 8 Hz, 2H; $SiCH_2$), 0.88 (t, J = 8Hz, 3H; CH_3), 1.22 (t, J = 8Hz, 6H; CH_3), 1.30–1.45 (m, 10H; CH_2), 1.75 (p, J = 8Hz, 2H; CH_2), 1.82 (p, J = 8Hz, 2H; CH_2), 3.78 (q, J = 8Hz, 4H; $SiOCH_2$), 4.21 (t, J = 8Hz, 4H; NCH_2), 8.68 (s, 4H; ArH).

Synthesis of 1,6,7,12-tetrachloro-N-octadecyl-N′-(dihydroxylmethylsilyl) propyl-perylene-3,4, 9,10-tetracarboxylic acid diimide: A mixture of 1,6,7,12-tetrachloro-*N-octadecyl*-N′-(dihydroxylmethylsilyl)propyl-perylene-3,4,9, 10-tetracarboxylic acid diimide (2.62 g), THF (300 mL), water (15 mL) and 1 M HCl (0.25 mL) was stirred for 4 h at room temperature. After that dichloromethane (200 mL) was added. The organic layer was washed with 60 ml of water three times and dried over Na_2SO_4. The solvent was removed and precipitated by n-hexane. A red solid was obtained (2.37 g, 97%). ^{1}H-NMR (400 MHz; $CDCl_3$; Me_4Si) δH (ppm): 0.26 (s, 3H;$SiCH_3$), 0.78 (t, J = 8 Hz, 2H; $SiCH_2$), 0.89 (t, J = 8Hz, 3H; CH_3), 1.30–1.45 (m, 10H; CH_2), 1.75 (p, J = 8Hz, 2H; CH_2), 1.94 (p, J = 8Hz, 2H; CH_2), 2.83 (s, 2H; SiOH), 4.24 (p, J = 8Hz, 4H; NCH_2), 8.70 (s, 4H; ArH).

Synthesis of PDISi: A mixture of 1,6,7,12-tetrachloro-*N*-octadecyl-*N′*-(dihydroxylmethylsilyl)propyl-perylene-3,4,9,10-tetracarboxylic acid diimide (2 g, 2.6 mmol), 1,6,7,12-tetrachloro-*N*-octadecyl-*N′*-(diethoxylmethylsilyl)propyl-perylene-3,4,9,10-tetracarboxylic acid diimide(2.15 g, 2.6 mmol), toluene (60 mL) and tetrabutyl titanate (0.2 mL) was heated to 40 °C for 7 days. After that, ethanol was added and the precipitate was collected by a filter as the product. ^{1}H-NMR (400 MHz; $CDCl_3$; Me_4Si) δH (ppm): 0.17 (s, 3H;SiCH3), 0.6–0.7 (2H; $SiCH_2$), 0.8–0.9 (3H; CH_3), 1.2–1.5 (10H; CH_2), 1.6–1.9 (4H; CH_2), 3.9–4.3 (4H; NCH_2), 8.2–8.7 (4H; ArH).

Synthesis of Methyl(5″-methyl-[2, 2′:5′, 2″-terthiophen]-5-yl) diethoxylsilane: A mixture of magnesium powder (0.24 g, 0.01 mol), THF (50 mL) and chlorodiethoxy(methyl)silane (1.68 g, 0.01 mol), was added to a 250 mL round flask. Then a solution of 3.41 g (0.01 mol) 5-bromo-5″-methyl-2, 2′:5′, 2″-terthiophene and 50 mL THF was added dropwise to the flask under stirring at reflux temperature for 2 h. A small amount of iodine was used to initiate the reaction. The reaction mixture was kept at reflux for 4 h. A brown liquid was obtained (2.13 g, 54%). ^{1}H-NMR (400 MHz; $CDCl_3$; Me_4Si) δH (ppm): 0.41 (s, 3H; $SiCH_3$), 1.26 (t, J = 7.2 Hz, 6H; CH_3), 2.48 (s, 3H; CH_3), 3.86 (q, J = 7.2 Hz,4H; CH_2), 6.67 (s, 1H; ArH), 6.97 (d, J = 6 Hz, 2H; ArH), 7.09 (d, J = 3.6 Hz, 1H; ArH), 7.22 (d, J = 3.6 Hz, 1H; ArH), 7.27 (d, J = 3.6 Hz, 1H; ArH).

Synthesis of Methyl(5″-methyl-[2, 2′:5′, 2″-terthiophen]-5-yl) dihydroxylsilane: A mixture of diethoxy(methyl)(5″-methyl-[2, 2′:5′, 2″-terthiophen]-5-yl)silane (1.5 g), THF (150 mL), water (10 mL) and 1 M HCl (0.2 mL) was stirred for 4 h at room temperature. After that dichloromethane (200 mL) was added. The organic layer was washed three times with 30 mL of water and dried over Na_2SO_4. The solvent was removed and precipitated by n-hexane. A yellow solid was obtained (1.22 g, 95%). ^{1}H-NMR (400 MHz; d_8-THF) δH (ppm): 0.25 (s, 3H; $SiCH_3$), 2.45 (s, 3H; CH_3), 5.75 (s, 2H; SiOH), 6.68 (d, J = 2.6 Hz, 1H; ArH), 6.99 (d, J = 3.6 Hz, 1H; ArH), 7.02 (d, J = 3.6 Hz, 1H; ArH), 7.10 (d, J = 3.6 Hz, 1H;ArH), 7.21–7.24 (m, 2H; ArH).

Synthesis of PTSi: A mixture of methyl(5″-methyl-[2, 2′:5′, 2″-terthiophen]-5-yl)diethoxylsilane (0.747 g, 1.9 mmol), methyl(5″-methyl-[2, 2′:5′, 2″-terthiophen]-5-yl)dihydroxylsilane (0.64 g, 1.9 mmol), THF (30 mL) and tetrabutyl titanate (0.2 mL) was heated to 40 °C for 5 days. After that, n-hexane was added and the precipitate was collected by a filter as the product. ^{1}H-NMR (400 MHz; $CDCl_3$; Me_4Si) δH (ppm): 0.40 (s, 3H; $SiCH_3$), 2.45 (s, 3H; CH_3), 6.5–7.3 (br, 6H; ArH).

Synthesis of PTSi-alt-PDISi: A mixture of methyl(5″-methyl-[2, 2′:5′, 2″-terthiophen]-5-yl)diethoxylsilane (1.2 g, 3 mmol), 1,6,7,12-tetrachloro-*N*-octadecyl-*N′*-(dihydroxylmethylsilyl)propyl-perylene-3,4,9,10-tetracarboxylic acid diimide (2.3 g, 3 mmol), toluene (50 mL) and tetrabutyl titanate (0.2 mL) was heated to 40 °C for 7 days. After that, ethanol was added and the precipitate was collected by a filter as the product. ^{1}H-NMR (400 MHz; $CDCl_3$; Me_4Si) δH (ppm): 0.1–0.3(3H;SiCH3), 0.3–0.5 (3H;SiCH3), 0.6–0.7 (2H; $SiCH_2$), 0.8–0.9 (3H; CH_3), 1.2–1.5 (10H; CH_2), 1.6–1.9 (4H; CH_2), 2–2.4 (3H; CH_3), 3.8–4.2 (4H; NCH_2), 6–7.2 (6H; ArH), 8.3–8.7 (4H; ArH).

Supporting Information

Supporting Information is available from the Wiley Online Library or from the author.

Acknowledgements

The financial support of NSFC (21104002 and 51221002) and Beijing Higher Education Young Elite Teacher Project (YETP0491) are gratefully acknowledged. Z.R. thanks the China Scholarship Council for funding a visit to Durham University.

Received: November 28, 2013
Published online: February 20, 2014

[1] S. Nadkarni, B. Yoo, D. Basu, A. Dodabalapur, *Appl. Phys. Lett.* **2006**, *89*, 184105.
[2] S. De Vusser, S. Steudel, K. Myny, J. Genoe, P. Heremans, *Appl. Phys. Lett.* **2006**, *88*, 162116.
[3] K. Hizu, T. Sekitani, T. Someya, J. Otsuki, *Appl. Phys. Lett.* **2007**, *90*, 093504.
[4] H. Klauk, U. Zschieschang, J. Pflaum, M. Halik, *Nature* **2007**, *445*, 745–748.
[5] Q. D. Ling, D. J. Liaw, E. Y. H. Teo, C. Zhu, D. S. H. Chan, E. T. Kang, K. G. Neoh, *Polymer* **2007**, *48*, 5182–5201.
[6] Q. D. Ling, D. J. Liaw, C. Zhu, D. S. H. Chan, E. T. Kang, K. G. Neoh, *Prog. Polym. Sci.* **2008**, *33*, 917–978.
[7] Y. Yang, J. Ouyang, L. Ma, R. J. H. Tseng, C. W. Chu, *Adv. Funct. Mater.* **2006**, *16*, 1001–1014.
[8] R. G. Hicks, *Nat. Chem.* **2011**, *3*, 189–191.
[9] P. Heremans, G. H. Gelinck, R. Muller, K. J. Baeg, D. Y. Kim, Y. Y. Noh, *Chem. Mater.* **2011**, *23*, 341–358.
[10] X. D. Zhuang, Y. Chen, B. X. Li, D. G. Ma, B. Zhang, Y. Li, *Chem. Mater.* **2010**, *22*, 4455–4461.
[11] Y. K. Fang, C. L. Liu, C. Li, C. J. Lin, R. Mezzenga, W. C. Chen, *Adv. Funct. Mater.* **2010**, *20*, 3012–3024.
[12] Q. D. Ling, Y. Song, S. L. Lim, E. Y. H. Teo, Y. P. Tan, C. Zhu, E. T. Kang, K. G. Neoh, *Angew. Chem., Int. Ed.* **2006**, *45*, 2947–2951.
[13] S. Baek, D. Lee, J. Kim, S. H. Hong, O. Kim, M. Ree, *Adv. Funct. Mater.* **2007**, *17*, 2637–2644.
[14] Y. K. Fang, C. L. Liu, W. C. Cheng, *J. Mater. Chem.* **2011**, *21*, 4778–4786.
[15] S. L. Lim, N. J. Li, J. M. Lu, Q. D. Ling, C. X. Zhu, E. T. Kang, K. G. Neoh, *ACS Appl. Mater. Interfaces* **2009**, *1*, 60–71.
[16] Q. D. Ling, F. C. Chang, Y. Sang, C. X. Zhu, D. J. Liaw, D. S. H. Chan, E. T. Kang, K. G. Neoh, *J. Am. Chem. Soc.* **2006**, *128*, 8732–8733.
[17] K. Kim, S. Park, S. G. Hahm, T. J. Lee, D. M. Kim, J. C. Kim, W. Kwon, Y. G. Ko, M. Ree, *J. Phys. Chem. B* **2009**, *113*, 9143–9150.
[18] N. H. You, C. C. Chueh, C. L. Liu, M. Ueda, W. C. Chen, *Macromolecules* **2009**, *42*, 4456–4463.
[19] K. L. Wang, Y. L. Liu, J. W. Lee, K. G. Neoh, E. T. Kang, *Macromolecules* **2010**, *43*, 7159–7164.
[20] G. F. Tian, D. Z. Wu, S. L. Qi, Z. P. Wu, X. D. Wang, *Macromol. Rapid Commun.* **2011**, *32*, 384–389.
[21] C. J. Chen, Y. C. Hu, G. S. Liou, *Polym. Chem.* **2013**, *4*, 4162–4171.
[22] Y. K. Fang, C. L. Liu, G. Y. Yang, P. C. Chen, W. C. Chen, *Macromolecules* **2011**, *44*, 2604–2612.
[23] E. Y. H. Teo, Q. D. Ling, Y. Song, Y. P. Tan, W. Wang, E. T. Kang, D. S. H. Chan, C. X. Zhu, *Org. Electron.* **2006**, *7*, 173–180.
[24] L. H. Xie, Q. D. Ling, X. Y. Hou, W. Huang, *J. Am. Chem. Soc.* **2008**, *130*, 2120–212.
[25] J. C. Scott, L. D. Bozano, *Adv. Mater.* **2007**, *19*, 1452–1463.

[26] D. Ma, M. Aguiar, J. A. Freire, I. A. Hümmelgen, *Adv. Mater.* **2000**, *12*, 1063–1066.
[27] Q. Ling, Y. Song, S. J. Ding, C. Zhu, D. S. H. Chan, D. L. Kwong, E. T. Kang, K. G. Neoh, *Adv. Mater.* **2005**, *17*, 455–459.
[28] Y. S. Lai, C. H. Tu, D. L. Kwong, J. S. Chen, *Appl. Phys. Lett.* **2005**, *87*, 122101.
[29] Q. Huang, G. A. Evmenenko, P. Dutta, P. Lee, N. R. Armstrong, T. J. Marks, *J. Am. Chem. Soc.* **2005**, *127*, 10227–10242.
[30] J. D. Froehlich, R. Young, T. Nakamura, Y. Ohmori, S. Li, A. Mochizuki, M. Lauters, G. E. Jabbour, *Chem. Mater.* **2007**, *19*, 4991–4997.
[31] Q. Zhou, S. Yan, C. C. Han, P. Xie, R. Zhang, *Adv. Mater.* **2008**, *20*, 2970–2976.
[32] F. Würthner, *Chem. Commun.* **2004**, 1564–1579.
[33] C. D. Dimitrakopoulos, P. R. L. Malenfant, *Adv. Mater.* **2002**, *14*, 99–117.
[34] X. Zhan, A. Facchetti, S. Barlow, T. J. Marks, M. A. Ratner, M. R. Wasielewski, S. R. Marder, *Adv. Mater.* **2011**, *23*, 268–284.
[35] B. Jancy, S. K. Asha, *J. Phys. Chem. B* **2006**, *110*, 20937–20947.
[36] T. Kurosawa, Y. C. Lai, T. Higashihara, M. Ueda, C. L. Liu, W. C. Chen, *Macromolecules* **2012**, *45*, 4556–4563.
[37] G. Zotti, G. Schiavon, A. Berlin, G. Pagani, *Chem. Mater.* **1993**, *5*, 430–436.
[38] S. Möller, C. Perlov, W. Jackson, C. Taussig, S. R. Forrest, *Nature* **2003**, *426*, 166–169.
[39] S. L. Lim, Q. D. Ling, E. Y. H. Teo, C. X. Zhu, D. S. H. Chan, E. T. Kang, K. G. Neoh, *Chem. Mater.* **2007**, *19*, 5148–5157.
[40] W. Kwon, B. Ahn, D. M. Kim, Y. G. Ko, S. G. Hahm, Y. Kim, H. Kim, M. Ree, *J. Phys. Chem. C* **2011**, *115*, 19355–19363.
[41] J. K. Choi, S. Jang, K. J. Kim, H. Sohn, H. D. Jeong, *J. Am. Chem. Soc.* **2011**, *133*, 7764–7785.
[42] S. J. Liu, P. Wang, Q. Zhao, H. Y. Yang, J. Wong, H. B. Sun, X. C. Dong,W. P. Lin, W. Huang, *Adv. Mater.* **2012**, *24*, 2901–2905.
[43] T. Kuorosawa, C. C. Chueh, C. L. Liu, T. Higashihara, M. Ueda, W. C. Chen, *Macromolecules* **2010**, *43*, 1236–1244.
[44] S. J. Liu, Z. H. Lin, Q. Zhao, Y. Ma, H. F. Shi, M. D. Yi, Q. D. Ling, Q. L. Fan, C. X. Zhu, E. T. Kang, W. Huang, *Adv. Funct. Mater.* **2011**, *21*, 979–985.
[45] D. Sun, Q. Fu, Z. Ren, W. Li, H. Li, D. Ma, S. Yan, *J. Mater. Chem. C* **2013**, *1*, 5344–5350.